Vol 18 No 7, July 2009
1674-1056/2009/18(07)/2734-05

Chinese Physics B

© 2009 Chin. Phys. Soc.
and IOP Publishing Ltd

X-ray absorption near the edge structure and x-ray photoelectron spectroscopy studies on pyrite prepared by thermally sulfurizing iron films*

Zhang Hui(张 辉)[a)b)†], Liu Ying-Shu(刘应书)[a)], Wang Bao-Yi(王宝义)[b)], Wei Long(魏 龙)[b)], Kui Re-Xi(奎热西)[b)], and Qian Hai-Jie(钱海杰)[b)]

[a)] *School of Mechanical Engineering, University of Science and Technology Beijing, Beijing* 100083, *China*

[b)] *Multidisciplinary Research Center, Chinese Academy of Sciences, Beijing* 100049, *China*

(Received 6 November 2008; revised manuscript received 17 November 2008)

This paper reports how pyrite films were prepared by thermal sulfurization of magnetron sputtered iron films and characterized by x-ray absorption near edge structure spectra and x-ray photoelectron spectroscopy on a 4B9B beam line at the Beijing Synchrotron Radiation Facility. The band gap of the pyrite agrees well with the optical band gap obtained by a spectrophotometer. The octahedral symmetry of pyrite leads to the splitting of the d orbit into t_{2g} and e_g levels. The high spin and low spin states were analysed through the difference of electron exchange interaction and the orbital crystal field. Only when the crystal field splitting is higher than 1.5 eV, the two weak peaks above the white lines can appear, and this was approved by experiments in the present work.

Keywords: x-ray absorption near the edge structure spectra, x-ray photoelectron spectroscopy, iron pyrite films, solar cells

PACC: 3365F, 7360F, 8115R

1. Introduction

Recently, iron pyrite (FeS_2), hereinafter referred to as pyrite, has been widely investigated because of its potential photovoltaic and photoeletrochemical applications stemming from its proper band gap and large absorption coefficient of $\alpha > 10^5$ cm^{-1} (for $\lambda < 700$ nm).[1,2] It is becoming a promising candidate, which can substitute for some solar materials, such as Si, CdTe, GaAs, and so on, due to its non-toxicity and abundant elements. Up to now, some techniques have been developed to produce pyrite thin films, such as sulfidation of iron and iron oxides,[3,4] reactive ion beam magnetron sputtering,[5] spray pyrolysis,[6] flash evaporation of pyrite powder,[7] sulphur-assisted magnetron sputtering,[8] screen print, chemical vapour transport and metal-organic chemical vapour deposition.[9,10] However, the values for the optical band gap, which depend mostly on the electronic structure, vary in a broad range from 0.7 to 2.62 eV with different manufacturing methods. Although experimental studies on the electronic structure of natural crystal[11] and theoretical calculations[12,13] based on density functional theory in local density approximation and generalized-gradient approximation have been performed, to our knowledge, seldom have papers been reported about the Fe and S $L_{2,3}$-edge of synthesized pyrite which can offer much information on the electronic structure and conduction bands.

Films described in this paper have been obtained by thermal sulfidation of metallic iron films sputtered on silicon and quartz substrates by magnetron sputtering. The aim of the present work is to investigate Fe and S $L_{2,3}$-edge x-ray absorption near edge structure (XANES) spectra by synchrotron radiation excited photoelectron spectroscopy and compare with the optical gap measured by a spectrophotometer.

2. Experiment

Pyrite films for this study have been obtained by thermally sulfurizing metallic iron films in sealed quartz ampoules. Generally, the rectangular substrates were boiled in a solution mixed with hydrochloric acid and sulfuric acid in a ratio of 3 to 1, and then rinsed with de-ionized water more than three times, and finally dried in a vacuum chamber at 423 K. Iron

*Project supported by the National Natural Science Foundation of China (Grant No 102750770).

†Corresponding author. E-mail: zhanghui56@me.ustb.edu.cn

films of about 200 nm were deposited on silicon and quartz substrates at room temperature in an FJL560 (made by the Shenyang Science Instrument Company, Shenyang, China) magnetron sputtering system. A base pressure of about 3.6×10^{-4} Pa was reached and a $\Phi 60 \times 2$ mm^2 iron target of nominal 99.9% purity was used. The iron films together with sulfur powder (99.5% of purity) were annealed in vacuum-sealed quartz ampoules of 20 mm diameter at 723 K for 20 hours.

The x-ray diffraction (XRD) experiments were performed at the diffuse–scattering station on a 4W1C beam line of the Beijing Synchrotron Radiation Facility (BSRF), using a Huber five-circle diffractometer, whose 2θ angular accuracy is nine arc seconds. The wavelength λ was 1.5406 Å. A focus spot size of 0.5 mm(H)×0.3 mm(V) with energy resolution of 4.4×10^{-4} and photon flux of 2×10^8 photons/s was obtained at the sample position. The incident angle θ was fixed at 5° and 2θ was scanned from 25° to 66° during the measurements.

The XANES spectra were recorded by total electron yield mode and the x-ray photoelectron spectroscopy (XPS) was characterized on a 4B9B beam line at BSRF. The storage ring was operated with electron energy of 2.2 G eV and a typical current of 100 mA was used during the experiment. The ultrahigh vacuum chamber background pressure was about 3×10^{-8} Pa and it was approximately 5×10^{-8} Pa during the measurements. The photon energies used to record the Fe, S L-edge absorption spectra ranged from 680 to 760 eV and 130 to 220 eV, respectively. The experimental resolution at these photon energies was estimated to be 0.3 eV.

The absorption spectra of the films at ambient temperature were recorded at optical wavelengths between 190 and 3200 nm with a UV-3100 spectrophotometer. The quartz substrate absorption was subtracted by placing a piece of bare quartz in the instrument reference channel.

3. Results and discussion

3.1. Surface XRD and optical properties

Figure 1(a) shows the surface XRD pattern of the pyrite on silicon substrate. In order to study the XPS and XANES spectra of the pyrite, iron films should be sputtered on silicon substrate other than glass to get an obvious electrical signal, but the silicon substrate would contribute a strong background to minimize the pyrite pattern in conventional XRD, so the surface XRD was used to get information from the pyrite layer. As can be seen, the incident x-ray was focused on pyrite with a $\theta = 5°$ to the surface. The sample was fixed while scanning. This method is different from conventional XRD which is $\theta-2\theta$ scanning. So the strong diffraction background from the silicon substrate can be eliminated. Pyrite patterns from the standard ASTM cards (ASTM 42-1340) are also plotted on the bottom of the figure for comparison. An average grain size of about 60 nm was computed from the full width at half maximum of each Miller index according to the Scherrer formula. This means that the crystallization of pyrite film was well done under the experimental conditions.

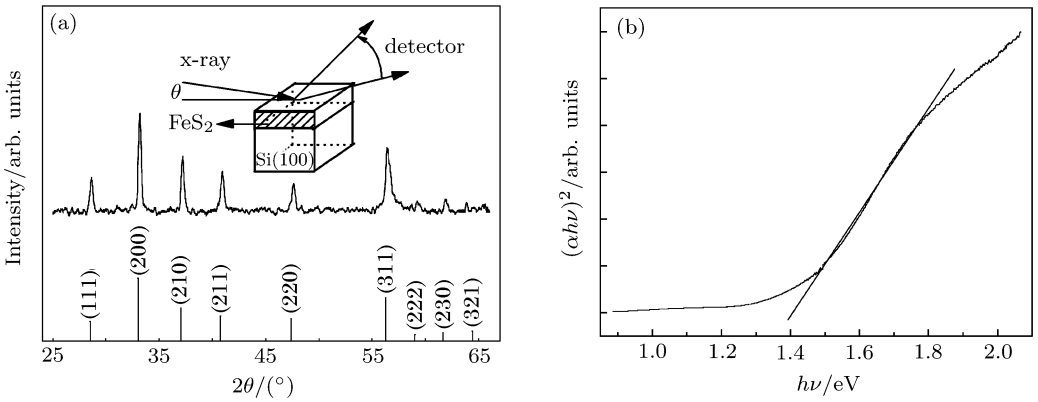


Fig.1. (a) Surface XRD pattern of the pyrite, (b) the optical gap of the pyrite.

Figure 1(b) shows the optical gap of the pyrite on the quartz substrate. The $(\alpha h\upsilon)^2 - h\upsilon$ curve of the sample was plotted according to the Tauc formula $(\alpha h\upsilon)^2 = A(h\upsilon - E_{\rm g})$, where α is the absorption coefficient, $h\upsilon$ is the energy of incident light quanta, A is a constant, and $E_{\rm g}$ is a parameter characterizing the electronic structure of the material. The optical gap can be obtained by extrapolation when $(\alpha h\upsilon)^2 = 0$. In this paper, the experimental data was fitted into linear regression line $y = ax + b$ by the least squares method. The optical gap of about 1.35 eV was calculated from the ratio of the intercept b and the slope a.

3.2. The XANES and XPS

Figures 2(b) and 2(d) show the XPS of Fe and S in pyrite, respectively. The XPS of Fe and S was calibrated by $C_{1\rm s}$ (284.6 eV). The binding energy of Fe and S can be obtained by the formula $E_{\rm b} = h\upsilon - \Phi_{\rm s}$, where $E_{\rm b}$ is the binding energy of the elements, $h\upsilon$ is the incident photon energy, $\Phi_{\rm s}$ is the work function of the equipment and $E_{\rm F}$ is the Fermi level. The information is listed in Table 1.

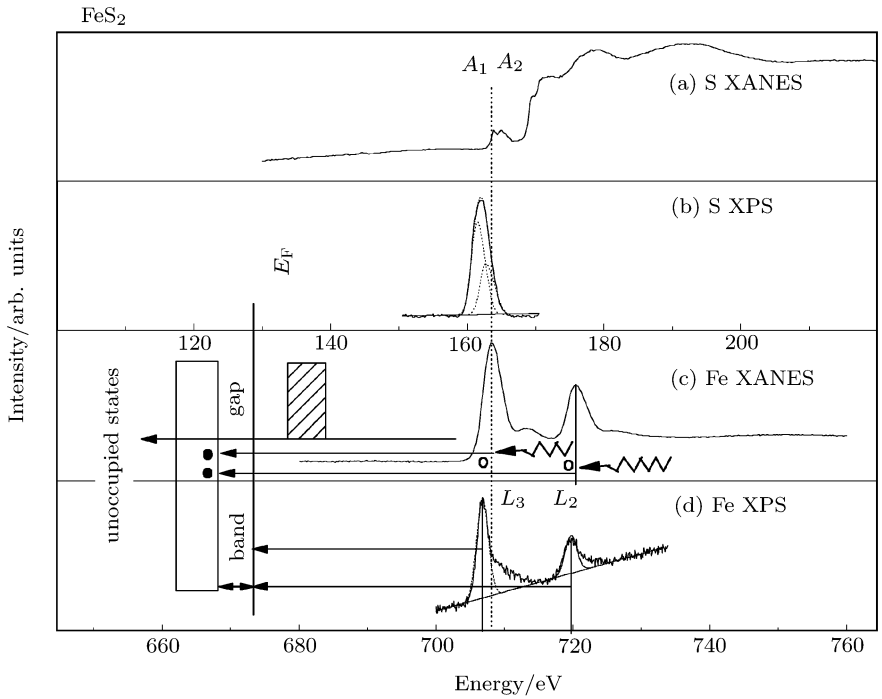


Fig.2. (a) The XANES of S $L_{2,3}$-edge, (b) binding energy of S2p$_{3/2}$ and S2p$_{1/2}$, (c) the XANES of Fe $L_{2,3}$-edge, (d) binding energy of Fe2p$_{3/2}$ and Fe2p$_{1/2}$ in pyrite.

Table 1. The binding energy of components from the pyrite.

compound	C	FeS_2				
chemical state	$C_{1\rm s}$	Fe2p$_{1/2}$	Fe2p$_{3/2}$	Fe3p	S2p$_{1/2}$	S2p$_{3/2}$
binding energy with $C_{1\rm s}$ calibration/eV	284.60	719.65	706.60	52.60	162.60	161.50

The XANES spectra are developed to deal with the electronic transitions from atomic core levels into unoccupied electronic states. Determination of the onset of x-ray absorption as a function of photon energy requires knowledge of the differences between the energies of the core electron states and the lowest unoccupied electronic states. Modifications to the final state of the electron arise when the outgoing electron emitted from a core level scatters the local surrounding atoms. The nature of the initial state from which the electron is emitted can also have a profound effect on the outgoing wave since this is created by a dipole transition process such that the angular momentum selection rules are obeyed, $\Delta l = \pm 1$, where l is the angular momentum quantum number.[14] Figures 2(a) and 2(c) shows the XANES of Fe and S in pyrite. We assign peak A_1, A_2 separated

by 1.1 eV at 162.90 eV and 164.00 eV to states at the minimum of the conduction band, which is related to the S $2p_{3/2}$, $2p_{1/2}$ spin–orbit splitting. The XPS results show that the binding energies of $S2p_{3/2}$ and $S2p_{1/2}$ are located at 161.5 eV and 162.6 eV, respectively, from which the fundamental gap is easily calculated to be 1.4 eV. This agrees well with the band gap obtained from optical measurements above. From the binding energies of Fe $2p_{3/2}$, $2p_{1/2}$ and the L_3 and L_2 absorption edge, the same value for the band gap was obtained.

3.3. The crystal structure and crystal field multiplet

3.3.1. Crystal structure

At room temperature FeS_2 crystallizes in the structure with space group *Pa3* (No. 205) and lattice constant $a = 0.5416$ nm as shown in Fig.3. Pyrite is akin to the rocksalt (NaCl) structure where Fe^{2+} is substituted for Na^+ and the centroid of the S_2^{2-} dimmer is located at Cl^- positions. These sulfur dumbbells S–S are oriented along the ⟨111⟩ axis. The

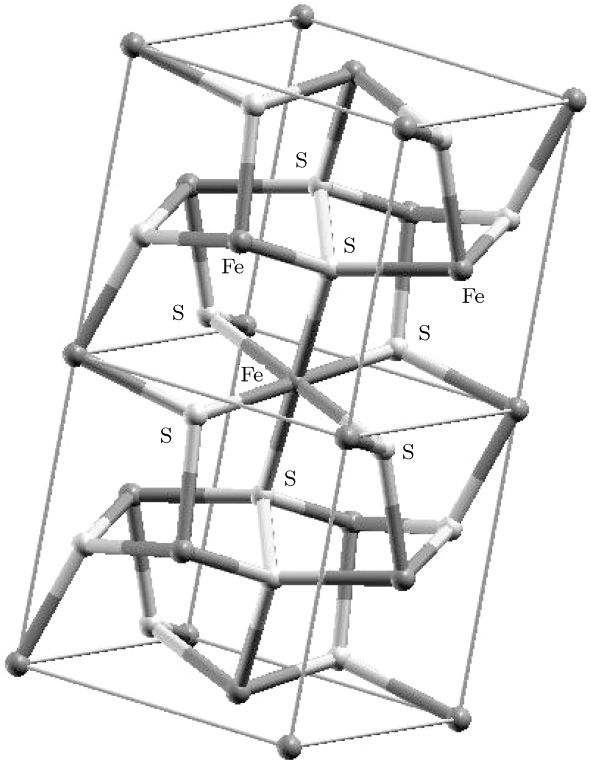


Fig.3. The crystal structure of FeS_2, iron and sulfur atoms is designated by dark solid balls and light gray balls, respectively.

Wyckoff positions Fe (4a): (0, 0, 0), (0, 1/2, 1/2), (1/2, 0, 1/2), (1/2, 1/2, 0) and S (8c): $\pm(u, u, u)$, $\pm(-u, 1/2 + u, 1/2 - u)$, $\pm(1/2 + u, 1/2 - u, -u)$, $\pm(1/2 - u, -u, 1/2 + u)$ are special cases of the general position (24d), Here u is the position parameter of sulfur and is equal to 0.387 from experimental measurements.[15] Six S atoms octahedrally coordinate each Fe atom whereas each S atom is tetrahedrally coordinated by three Fe atoms (S–Fe bond length = 0.2265 nm) and one S atom (S–S bond length = 0.2161 nm). They form a so-called octahedral field, which belongs to the O_h point group. Consequently, the symmetry changes from spherical symmetry (SO_3) to octahedral symmetry (O_h), and this leads to the D symmetry state branching to E_g and T_{2g} symmetry states.

3.3.2. Crystal field multiplet

For the configurations $3d^6$ in pyrite, there are two possible ground state configurations in O_h symmetry. One is the high-spin ground state which originates from Hund's rule; the other is the low-spin ground state in which all t_{2g} levels are filled with electrons. Figure 4 gives the high-spin and low-spin occupations of the t_{2g} and e_g. The transition point from high-spin to low-spin ground states is determined by the crystal field $10D_q$ and the exchange splitting J. In the high spin state, there are two electrons jumping from low-level t_{2g} to high level e_g, so the crystal field splitting $2D$ is the difference of the two kinds of configuration. While for the exchange interaction, the exchange splitting is presented for every two parallel electrons. In the high spin state, the exchange splitting is $J_{ee}(\uparrow) + 3J_{tt}(\uparrow) + 6J_{te}(\uparrow)$, and $3J_{tt}(\uparrow) + 3J_{tt}(\downarrow)$ for the low spin state. Here J_{ee}, J_{tt}, J_{te} represent two electrons in e_g, t_{2g}, e_g and t_{2g} orbital, respectively, so the J difference between high spin and low spin is $6J_{te} + J_{ee} - 3J_{tt}$. Figure 4 contains the overall exchange interactions and can estimate the transition point. For estimation, the exchange splitting was assumed to be equal. Low spin states for Fe $3d^6$ configurations are found if the crystal field splitting is more than $2J$. Because J can be estimated as 0.8 eV, the transition points are approximately 1.6 eV for Fe $3d^6$. In other words, Fe $3d^6$ materials have a tendency to be low-spin compounds. This is particularly true for Fe $3d^6$ compounds because of the additional stabilizing nature of the $3d^6$ $^1A_{1g}$ low spin ground state.[16]

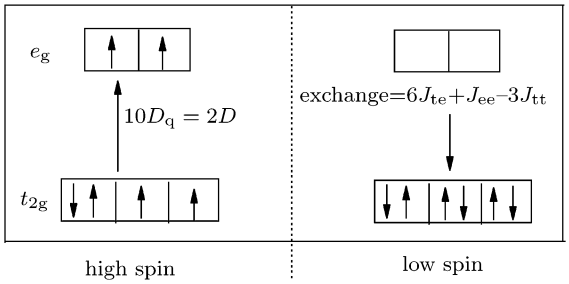


Fig.4. Two kinds of configuration for high spin and low spin in O_h symmetry.

Figure 5 shows the experimental and computational results of the Fe $L_{2,3}$-edge in pyrite. The Cowan Program[17] was used for calculation in the present work. Figure 5(a) is the spectrum of the Fe $L_{2,3}$-edge while the crystal field strength is 1.0 (0.304 eV). Two main peaks for Fe L_3 and L_2 due to spin–orbit splitting are observed. When the crystal field length increases to 5.0 (1.5 eV), there are two weak peaks appearing above the corresponding ones. Just as seen in the bottom of Fig.5, the experimental results show that peaks a_2 and b_2 appear about 5.2 eV above L_3 and L_2, respectively, with low intensity. This is consistent with Cowan programming results. So we can conclude that the two weak peaks appear only when the crystal field length is greater than 1.5 eV. This fact agrees well with the analysis in low spin states. Also we know that pyrite is a kind of anti-ferromagnetic semiconductor and seldom paired electrons exist in the material.

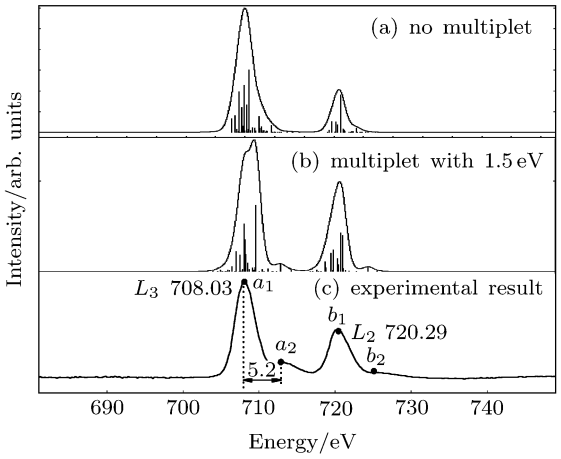


Fig.5. The experimental and calculated results of the Fe $L_{2,3}$-edge in pyrite.

4. Conclusions

The Fe and S $L_{2,3}$ XANES and XPS spectra of synthesized pyrite were characterized by synchrotron radiation excited photoelectron spectroscopy. The optical band gap measured by a spectrophotometer accords well with the band gap obtained by XANES. An unoccupied state exists about 1.4 eV above the Fermi level. The octahedral symmetry of pyrite leads to the splitting of the d orbital. Only when the crystal field splitting is higher than 1.5 eV, the two weak peak above the white lines can appear, and this was proved by experiments in the present work.

References

[1] Ennaoui A, Fiechter S and Goslowsky H 1985 *J. Electrochem. Soc.* **132** 1579
[2] Ferrer I J, Nevskaia D M, de las Heras C and Sanchez C 1990 *Solid State Commun.* **74** 913
[3] Smestad G, Ennaoui A, Fiechter S, Tributsh H, Hofmann W K, Birkholz M and Kautek W 1990 *Sol. Energy Mater.* **20** 149
[4] Wan D Y, Wang Y T, Wang B Y, Ma C X, Sun H and Wei L 2003 *J. Cryst. Growth* **253** 230
[5] Pan M X, Cao X Z, Li Y X, Wang B Y, Xue D S, Ma C X, Zhou C L and Wei L 2004 *Acta Phys. Sin.* **53** 1956 (in Chinese)
[6] Thomas B, Ellmer K and Muller M 1997 *J. Cryst. Growth* **170** 808
[7] de las Heras C and Sanchez C 1991 *Thin Solid Films* **199** 259
[8] Willeke G, Dasbach K, Sailer B and Bucher E 1992 *Thin Solid Films* **213** 271
[9] Chatzitheodorou G, Fiechter S, Konenkamp R, Kunst M, Jaegermann W and Tributsch H 1986 *Mater. Res. Bull.* **21** 1481
[10] Schleich D M and Chang H S 1991 *J. Cryst. Growth* **112** 737
[11] Mattila S, Leiro J A and Laajalehto K 2003 *Appl. Surf. Sci.* **212–213** 97
[12] Eyert V, Höck K H and Fiechter S 1998 *Phys. Rev.* B **57** 6350
[13] Andrew H, Joseph M and Irene Y 2002 *Surf. Sci.* **513** 511
[14] de Groot F M F 2001 *Chem. Rev.* **101** 1779
[15] Finklea S, Cathey L and Amma E 1976 *Acta Crystallogr.* **32** 529
[16] Thole B T, Cowan R D, Sawatzky G A, Fink J and Fuggle J C 1985 *Phys. Rev.* B **31** 6856
[17] de Groot F 2004 *Coord. Chem. Rev.* **249** 31 (in Chinese)